Fourier-transform photoluminescence spectroscopy of excitons bound to group-III acceptors in silicon: Uniaxial stress

V. A. Karasyuk, M. L. W. Thewalt, and S. An
Department of Physics, Simon Fraser University, Burnaby, British Columbia, Canada V5A 1S6

E. C. Lightowlers
Physics Department, King's College London, Strand, London WC2R 2LS, United Kingdom

(Received 6 August 1997)

Photoluminescence of excitons bound to Al, Ga, In, and Tl acceptors in Si crystals subjected to ⟨001⟩, ⟨111⟩, or ⟨110⟩ uniaxial stress was studied at liquid-He temperatures with 0.0025-meV spectral resolution. The deformation-potential constants of the group-III acceptors in the ground state are (in eV) $b=-1.01\pm0.02$, $d=-3.31\pm0.06$ for Al, $b=-1.03\pm0.02$, $d=-3.10\pm0.06$ for Ga, $b=-0.43\pm0.01$, $d=-2.41\pm0.05$ for In, and $b=-0.30\pm0.03$, $d=-1.95\pm0.2$ for Tl. The shear deformation-potential constant for electrons in acceptor bound excitons $\Xi_u=8.6$ eV for all group-III acceptors within an experimental error of ±0.15 eV for Al, Ga, and In, and ±0.8 eV for Tl. The order of the valley-orbit states in Tl bound excitons is Γ_1, Γ_3, Γ_5 with the Γ_5 energy 1.21 meV above Γ_1, and 0.10 meV above Γ_3. All details of the spectra including positions, relative amplitudes, and polarizations of the components have been explained on the basis of a simple model of acceptor bound excitons with holes in the $J=0$ state taking into account the valley-orbit splitting and the spin-orbit coupling of the electron. Significant deviations from the theoretical predictions were observed only for very small strains producing acceptor splittings comparable with the intrinsic zero-stress splitting. [S0163-1829(97)01247-2]

I. INTRODUCTION

In our previous paper,[1] we have studied photoluminescence (PL) spectra of excitons bound to group-III shallow acceptors (A^0X, where A^0 stands for a particular acceptor species in its neutral state) in monocrystalline silicon in magnetic fields up to 14.5 T with a spectral resolution of 0.0025 meV. In the present paper, we report the results of similar studies in Si under uniaxial stress. Elastic deformation caused by stress induces changes in the electronic states of A^0X and A^0 reflected in the PL spectra. These changes can be described by means of perturbation theory and provide additional information on the symmetry and the structure of A^0X and A^0.

PL spectra of A^0X in nonperturbed Si exhibit an extended fine structure due to the valley-orbit splitting (VOS) and the spin-orbit coupling (SOC) in A^0X, and the intrinsic ground-state splitting Δ_0 of A^0.[1] Employment of a spectrometer with the ultrahigh resolution of 0.0025 meV and an advanced uniaxial stress technique[2] has allowed us to resolve this fine structure in the PL spectra of A^0X under uniaxial stress, which sets apart the present work from the previous uniaxial stress studies of A^0X.[3–8] Among them, only one, by Weber, Conzelman, and Sauer,[5] has dealt with In^0X and Tl^0X at about a hundred times lower resolution, not sufficient to resolve the VOS. The case of boron was explored earlier[9] in great detail, and in the present work we are concerned with the rest of the group-III acceptors Al, Ga, In, and Tl. We have already reported some of the results of ultrahigh-resolution piezospectroscopy of Al^0X and Ga^0X with regard to Δ_0.[10,11]

II. THEORY

A. Effect of elastic uniaxial strains on A^0

We are following here the same theoretical treatment of A^0X and A^0 as we did in the first part of this study[1] with the appropriate replacement of the magnetic-field perturbation with the elastic strain perturbation. Due to the lack of a theoretical model for the intrinsic ground-state splitting of A^0, we shall neglect it and describe the ground state of A^0 in Si as a quadruplet of the effective-mass states with a $1S$-type envelope function multiplied by the Bloch functions corresponding to the top of the valence band Γ_8^+. We use the same basis of four functions ψ_μ ($\mu=+\frac{3}{2},+\frac{1}{2},-\frac{1}{2},-\frac{3}{2}$) as we did in Ref. 1, labeled by the subscript μ equal to the projection m_j of the angular momentum **j** on the [001] axis. The effect on A^0 of the elastic strain represented by the strain tensor ε_{ij} can be described in this basis by the perturbation matrix[12]

$$\hat{H}(\varepsilon_{ij})=a\sum_i \varepsilon_{ii}+b\sum_i \varepsilon_{ii}(J_i^2-\tfrac{1}{3}J^2)+\frac{2d}{\sqrt{3}}\sum_{i<j}\varepsilon_{ij}\{J_iJ_j\},$$

$$\{J_iJ_j\}\equiv\tfrac{1}{2}(J_iJ_j+J_jJ_i),\quad J^2=J_x^2+J_y^2+J_z^2, \tag{1}$$

where the constants a, b, and d are the deformation potentials, and J_i ($i=x,y,z$) are the angular momentum matrices [Eq. (3) of Ref. 1]. Uniaxial stress with force **F** applied along an axis with direction cosines α_x, α_y, and α_z splits the quadruplet Γ_8 into two Kramers doublets separated by the energy Δ given by[12]

$$\Delta^2(\alpha_x,\alpha_y,\alpha_z)=\Delta_{001}^2+3(\Delta_{111}^2-\Delta_{001}^2)K(\alpha_x,\alpha_y,\alpha_z),$$

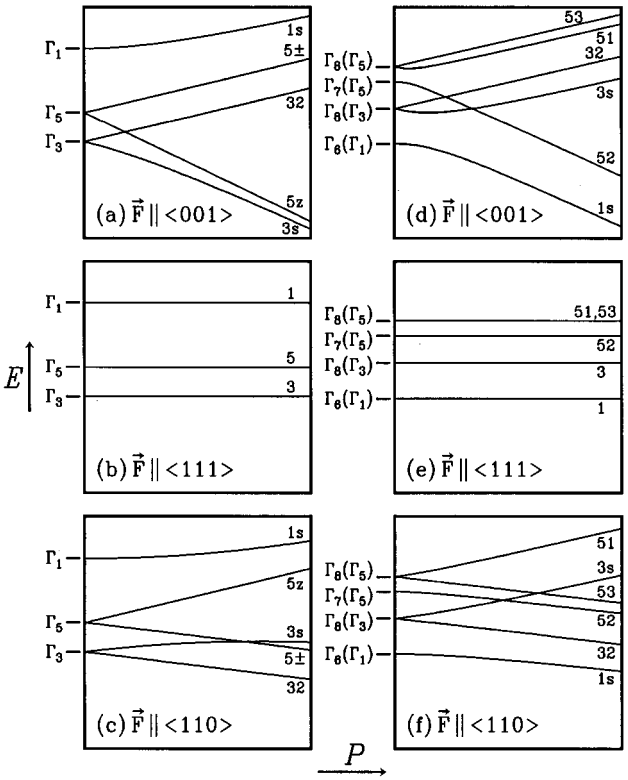

FIG. 1. The VOS of the acceptor bound exciton (A^0X) energy levels as a function of uniaxial stress P (compression) along the $\langle 001\rangle$ (a), (d), $\langle 111\rangle$ (b), (e), and $\langle 110\rangle$ (c), (f) crystallographic axes. Horizontal marks show the A^0X energy levels at $P=0$ with (d)–(f) and without (a)–(c) the SOC labeled by the corresponding irreducible representations of the point group T_d. The ordering of the VO states in (a)–(c) corresponds to that of Al^0X or Ga^0X, while (d)–(f) corresponds to that of In^0X. The energy levels are labeled on the right-hand side according to Eqs. (7) and (10)–(15) in the text.

$$K(\alpha_x,\alpha_y,\alpha_z)=\alpha_x{}^2\alpha_y{}^2+\alpha_y{}^2\alpha_z{}^2+\alpha_z{}^2\alpha_x{}^2. \tag{2}$$

Here $\Delta_{001}=2b(S_{11}-S_{12})T$ and $\Delta_{111}=(d/\sqrt{3})S_{44}T$ are the energy separations of the doublets for $\mathbf{F}\|\langle 001\rangle$ and $\mathbf{F}\|\langle 111\rangle$, respectively, where $S_{11}=0.7617\times10^{-11}$ m^2/N, $S_{12}=-0.2127\times10^{-11}$ m^2/N, and $S_{44}=1.2463\times10^{-11}$ m^2/N are the elastic compliance coefficients for Si,[13] and T is the magnitude of the stress which is negative for compression. For $\mathbf{F}\|\langle 110\rangle$, $\Delta^2=\Delta_{110}^2=\frac{1}{4}(\Delta_{001}^2+3\Delta_{111}^2)$. The median of the doublets is shifted by the same amount

$$\Delta E_{\rm hs}^{A^0}=a(S_{11}+2S_{12})T \tag{3}$$

for any direction of $\mathbf{F}$. The eigenfunctions of A^0 under uniaxial stress can be found in Ref. 14.

B. Effect of elastic uniaxial strains on A^0X

For all the group-III shallow acceptors in Si except for boron, the A^0X two-hole state with the net angular momentum $J=0$ (Γ_1) has a significantly lower energy than the state $J=2$ which is split by the crystal field into the states Γ_3 and Γ_5.[4] Only the state Γ_1 of Al^0X, Ga^0X, In^0X, and Tl^0X is populated at liquid-He temperatures. The state Γ_1 is a spin singlet and holes in this state do not couple to the electron, therefore, in the first approximation, the energy levels of A^0X can be obtained as the sum of the single-electron and the two-hole energy levels.

Uniaxial strains do not split the state Γ_1, but mix it with the states Γ_3 and Γ_5 resulting in a nonlinear redshift $\Delta E^{\rm hh}$ of the state Γ_1. Neglecting a relatively weak electron-hole coupling, $\Delta E^{\rm hh}$ can be expressed as a function of the stress splitting $\tilde{\Delta}$ of the single hole states of A^0X given by Eq. (2) with the A^0X values of the deformation-potential constants b and d which can differ from the values of b and d for A^0, and the zero stress separations $\Delta_{31}^{\rm hh}=E(\Gamma_3)-E(\Gamma_1)$ and $\Delta_{51}^{\rm hh}=E(\Gamma_5)-E(\Gamma_1)$ between the energy levels of the two-hole states Γ_3 and Γ_5, respectively, and the state Γ_1:

$$\Delta E^{\rm hh}=2a(S_{11}+2S_{12})T+\frac{\Delta_3^{\rm hh}}{2}-\sqrt{\left(\frac{\Delta_3^{\rm hh}}{2}\right)^2+\tilde{\Delta}^2} \tag{4}$$

for $\mathbf{F}\|\langle 001\rangle$, and

$$\Delta E^{\rm hh}=2a(S_{11}+2S_{12})T+\frac{\Delta_5^{\rm hh}}{2}-\sqrt{\left(\frac{\Delta_5^{\rm hh}}{2}\right)^2+\tilde{\Delta}^2} \tag{5}$$

for $\mathbf{F}\|\langle 111\rangle$. For $\mathbf{F}\|\langle 110\rangle$, $\Delta E^{\rm hh}=2a(S_{11}+2S_{12})T+E_1$, where E_1 is equal to the lowest root of the equation:

$$E(E-\Delta_{51}^{\rm hh})(E-\Delta_{31}^{\rm hh})+\frac{1}{4}\tilde{\Delta}^2(E-\Delta_{51}^{\rm hh})+\frac{3}{4}\tilde{\Delta}^2(E-\Delta_{31}^{\rm hh})=0. \tag{6}$$

The single-electron energy levels and the eigenstates for the uniaxial stress with $\mathbf{F}$ lying in the (110) plane at an angle θ with respect to the [001] axis can be obtained by diagonalization of the single-electron Hamiltonian which in the basis of the products of the functions[1]

$$\phi^{(1)}=\frac{1}{\sqrt{6}}\,(111\overline{111}) \quad :\Gamma_1,$$

$$\left.\begin{aligned}\phi^{(31)}&=\frac{1}{2\sqrt{3}}\,(\overline{111}12)\\ \phi^{(32)}&=\frac{1}{2}\,(11\overline{1}00)\end{aligned}\right\} \quad :\Gamma_3,$$

$$\left.\begin{aligned}\phi^{(5+)}&=\frac{1}{\sqrt{2}}\,(\phi^{(5x)}+i\phi^{(5y)})=\frac{1}{2}\,(1\overline{1}ii00)\\ \phi^{(5-)}&=\frac{1}{\sqrt{2}}\,(\phi^{(5x)}-i\phi^{(5y)})=\frac{1}{2}\,(1\overline{1}\overline{ii}00)\\ \phi^{(5z)}&=\frac{1}{\sqrt{2}}\,(000011)\end{aligned}\right\} \quad :\Gamma_5, \tag{7}$$

and the spinors $|\alpha\rangle$ and $|\beta\rangle$, has the form

TABLE I. Relative probabilities of the optical transitions from A^0X with holes in the lowest two-hole state and electron in the VO state $\psi^{(n)}$ [Eqs. (10)–(15)] to the upper (u) and the lower (l) sublevels of A^0 split by the [001] uniaxial compression of the sample. Light is emitted perpendicular to the stress axis with polarization perpendicular to the stress axis. η, γ, λ-independent constants (Ref. 1).

$\psi_e^{(n)}$	$u(\lvert m_j\rvert=\frac{3}{2})$	$l(\lvert m_j\rvert=\frac{1}{2})$
1σ	$\frac{1-\kappa}{3}\left[\sqrt{(1+\xi)}(2\eta+\lambda)-\frac{x}{\lvert x\rvert}\sqrt{\frac{1-\xi}{2}}(\eta-\lambda)\right]^2$	$\frac{1+\kappa}{9}\left[\sqrt{(1+\xi)}(2\eta+\lambda)-\frac{x}{\lvert x\rvert}\sqrt{\frac{1-\xi}{2}}(\eta-\lambda)\right]^2$
3σ	$\frac{1-\kappa}{3}\left[\frac{x}{\lvert x\rvert}\sqrt{(1-\xi)}(2\eta+\lambda)+\sqrt{\frac{1+\xi}{2}}(\eta-\lambda)\right]^2$	$\frac{1+\kappa}{9}\left[\frac{x}{\lvert x\rvert}\sqrt{(1-\xi)}(2\eta+\lambda)+\sqrt{\frac{1+\xi}{2}}(\eta-\lambda)\right]^2$
32	$(1-\kappa)(\eta-\lambda)^2$	$\frac{1+\kappa}{3}(\eta-\lambda)^2$
$51(5\pm)$	$(1-\kappa)(1+\zeta)\gamma^2$	$\frac{1+\kappa}{3}[\sqrt{2(1-\zeta)}-\sqrt{1+\zeta}]^2\gamma^2$
$52(5z)$	$(1-\kappa)(1-\zeta)\gamma^2$	$\frac{1+\kappa}{3}[\sqrt{2(1+\zeta)}+\sqrt{1-\zeta}]^2\gamma^2$
$53(5\pm)$	0	$\frac{4}{3}(1+\kappa)\gamma^2$

$$\kappa=\left[\frac{\left(\frac{2\tilde{\Delta}_{001}}{\Delta_{31}^{\mathrm{hh}}}\right)^2}{1+\left(\frac{2\tilde{\Delta}_{001}}{\Delta_{31}^{\mathrm{hh}}}\right)^2}\right]^{1/2},\quad x=\frac{\Xi_u(S_{11}-S_{12})T}{3\Delta_{31}^{\mathrm{VO}}},\quad \xi=\frac{1+x}{\sqrt{1+2x+9x^2}},$$

$$y=\frac{\Xi_u(S_{11}-S_{12})T}{3\lambda^{\mathrm{SO}}},\quad \zeta=\frac{1+6y}{3\sqrt{1+\frac{4}{3}y+4y^2}}$$

$$\hat{H}^e=\Delta E_{\mathrm{hs}}^e+\begin{bmatrix}\Delta_{15}^{\mathrm{VO}} & \sqrt{2}\sigma & 0 & 0 & 0 & 0\\ \sqrt{2}\sigma & \Delta_{35}^{\mathrm{VO}}+\sigma & 0 & 0 & 0 & 0\\ 0 & 0 & \Delta_{35}^{\mathrm{VO}}-\sigma & 0 & 0 & 0\\ 0 & 0 & 0 & -\sigma & 0 & 0\\ 0 & 0 & 0 & 0 & -\sigma & 0\\ 0 & 0 & 0 & 0 & 0 & 2\sigma\end{bmatrix}\otimes\begin{bmatrix}1 & 0\\ 0 & 1\end{bmatrix}+\frac{\lambda^{\mathrm{SO}}}{2}\begin{bmatrix}0 & 0\\ 0 & 1\end{bmatrix}\otimes\begin{bmatrix}1 & 0 & 0 & 0 & 0 & 0\\ 0 & -1 & 0 & 0 & -\sqrt{2} & 0\\ 0 & 0 & -1 & 0 & 0 & \sqrt{2}\\ 0 & 0 & 0 & 1 & 0 & 0\\ 0 & -\sqrt{2} & 0 & 0 & 0 & 0\\ 0 & 0 & \sqrt{2} & 0 & 0 & 0\end{bmatrix}, \tag{8}$$

$$\sigma\equiv\frac{1}{6}\Xi_u(S_{11}-S_{12})T(3\cos^2\theta-1),$$

$$\Delta E_{\mathrm{hs}}^e=\left(\Xi_d+\frac{1}{3}\Xi_u\right)(S_{11}+2S_{12})T. \tag{9}$$

Here, $\Delta_{15}^{\mathrm{VO}}$ and $\Delta_{35}^{\mathrm{VO}}$ are the energy separations of the VO states Γ_1 and Γ_3, respectively, from the VO states Γ_5 in the absence of stress and SOC, Ξ_d and Ξ_u are the dilational and shear deformation-potential constants,[12] and λ^{SO} is the SOC constant. We assume that $\Delta_{35}^{\mathrm{VO}}\gg\lambda^{\mathrm{SO}}$, and neglect the effect of SOC on the Γ_3 states.[1] The single-electron energy levels and the corresponding eigenfunctions can be expressed in a simple analytical form:

$$E_{1\sigma}=\Delta E_{\mathrm{hs}}^e+\Delta_{15}^{\mathrm{VO}}+\frac{\Delta_{31}^{\mathrm{VO}}}{2}(1+x-\sqrt{1+2x+9x^2}),$$

$$\phi^{(1\sigma)}=\frac{1}{\sqrt{2}}\left(\sqrt{1+\xi}\phi^{(1)}-\frac{x}{\lvert x\rvert}\sqrt{1-\xi}\phi^{(31)}\right), \tag{10}$$

$$E_{3\sigma}=\Delta E_{\mathrm{hs}}^e+\Delta_{15}^{\mathrm{VO}}+\frac{\Delta_{31}^{\mathrm{VO}}}{2}(1+x+\sqrt{1+2x+9x^2}),$$

$$\phi^{(3\sigma)}=\frac{1}{\sqrt{2}}\left(\frac{x}{\lvert x\rvert}\sqrt{1-\xi}\phi^{(1)}+\sqrt{1+\xi}\phi^{(31)}\right), \tag{11}$$

TABLE II. Relative probabilities of the optical transitions from A^0X with holes in the lowest two-hole state and electron in the VO state $\psi^{(n)}$ to the upper (u) and the lower (l) sublevels of A^0 split by the [001] uniaxial compression of the sample. Light is emitted perpendicular to the stress axis with polarization parallel to the stress axis.

$\psi_e^{(n)}$	$u(\lvert m_j\rvert=\frac{3}{2})$	$l(\lvert m_j\rvert=\frac{1}{2})$
1σ	0	$\frac{4}{9}(1+\kappa)\left[\sqrt{1+\xi}(2\eta+\lambda)-\frac{x}{\lvert x\rvert}\sqrt{2(1-\xi)}(\eta-\lambda)\right]^2$
3σ	0	$\frac{4}{9}(1+\kappa)\left[\frac{x}{\lvert x\rvert}\sqrt{1-\xi}(2\eta+\lambda)+\sqrt{2(1+\xi)}(\eta-\lambda)\right]^2$
32	0	0
$51(5\pm)$	$2(1-\kappa)(1-\zeta)\gamma^2$	0
$52(5z)$	$2(1-\kappa)(1+\zeta)\gamma^2$	0
$53(5\pm)$	0	$\frac{4}{3}(1+\kappa)\gamma^2$

$$\Delta_{31}^{\mathrm{VO}}\equiv\Delta_{35}^{\mathrm{VO}}-\Delta_{15}^{\mathrm{VO}},\quad x\equiv\frac{\sigma}{\Delta_{31}^{\mathrm{VO}}},\quad \xi\equiv\frac{1+x}{\sqrt{1+2x+9x^2}},$$

$$E_{32}=\Delta E_{\mathrm{hs}}^{e}+\Delta_{35}^{\mathrm{VO}}-\sigma,\quad \phi^{(32)}; \tag{12}$$

$$E_{51}=\Delta E_{\mathrm{hs}}^{e}-\frac{\lambda^{\mathrm{SO}}}{4}(1-2y-3\sqrt{1+\tfrac{4}{3}\,y+4y^2}),$$

$$\psi_e^{(51+)}=\frac{1}{\sqrt{2}}(\sqrt{1-\zeta}\,\phi^{(5+)}|\beta\rangle-\sqrt{1+\zeta}\,\phi^{(z)}|\alpha\rangle),$$

$$\psi_e^{(51-)}=\frac{1}{\sqrt{2}}(\sqrt{1-\zeta}\,\phi^{(5-)}|\alpha\rangle+\sqrt{1+\zeta}\,\phi^{(z)}|\beta\rangle), \tag{13}$$

$$E_{52}=\Delta E_{\mathrm{hs}}^{e}-\frac{\lambda^{\mathrm{SO}}}{4}(1-2y+3\sqrt{1+\tfrac{4}{3}y+4y^2}),$$

$$\psi_e^{(52+)}=\frac{1}{\sqrt{2}}(\sqrt{1+\zeta}\,\phi^{(5+)}|\beta\rangle+\sqrt{1-\zeta}\,\phi^{(z)}|\alpha\rangle),$$

$$\psi_e^{(52-)}=\frac{1}{\sqrt{2}}(\sqrt{1+\zeta}\,\phi^{(5-)}|\alpha\rangle-\sqrt{1-\zeta}\,\phi^{(z)}|\beta\rangle), \tag{14}$$

$$y\equiv\frac{\sigma}{\lambda^{\mathrm{SO}}},\quad \zeta\equiv\frac{1+6y}{3\sqrt{1+\frac{4}{3}y+4y^2}},$$

$$E_{53}=\Delta E_{\mathrm{hs}}^{e}+\frac{\lambda^{\mathrm{SO}}}{2}-\sigma,\quad \psi_e^{(53+)}=\phi^{(5+)}|\alpha\rangle,$$

$$\psi_e^{(53-)}=\phi^{(5-)}|\beta\rangle. \tag{15}$$

Each of the eigenfunctions in Eqs. (10)–(12) must be multiplied by a spinor $|\alpha\rangle$ or $|\beta\rangle$. The Γ_5 energy level E_{51} merges in the absence of stress with the level E_{53} and the corresponding eigenfunctions $\psi_e^{(51+)}$ and $\psi_e^{(51-)}$ together with the eigenfunctions $\psi_e^{(53+)}$ and $\psi_e^{(53-)}$ form the basis of the Γ_8 representation while the functions $\psi_e^{(52+)}$ and $\psi_e^{(52-)}$ form the basis of Γ_7. The evolution of the single energy levels with the increasing uniaxial compression for two representative cases of Al^0X and In^0X is shown in the Fig. 1.

TABLE III. Relative probabilities of the optical transitions from A^0X with holes in the lowest two-hole state and electron in the specified VO state to the upper (u) and the lower (l) sublevels of A^0 split by the [111] uniaxial compression of the sample. Light is emitted perpendicular to the stress axis with polarization perpendicular to the stress axis.

VO state	$u(\lvert m_j'\rvert=\frac{3}{2})$	$l(\lvert m_j'\rvert=\frac{1}{2})$
$\Gamma_6(\Gamma_1)$	$\frac{2}{3}(1-\kappa)(2\eta+\lambda)^2$	$\frac{2}{9}(1+\kappa)(2\eta+\lambda)^2$
$\Gamma_8(\Gamma_3)$	$\frac{2}{3}(1-\kappa)(\eta-\lambda)^2$	$\frac{10}{9}(1+\kappa)(\eta-\lambda)^2$
$\Gamma_7(\Gamma_5)$	$2(1-\kappa)\gamma^2$	$\frac{2}{3}(1+\kappa)\gamma^2$
$\Gamma_8(\Gamma_5)$	$\frac{4}{3}(1-\kappa)\gamma^2$	$\frac{4}{3}(1+\kappa)\gamma^2$

$$\kappa=\left[\frac{\left(\frac{2\tilde{\Delta}_{111}}{\Delta_{51}^{\mathrm{hh}}}\right)^2}{1+\left(\frac{2\tilde{\Delta}_{111}}{\Delta_{51}^{\mathrm{hh}}}\right)^2}\right]^{1/2}$$

C. Relative probabilities of optical transitions

The relative probabilities of the optical transitions from A^0X with holes in the lowest two-hole state and electron in the VO state $\psi^{(n)}$ [Eqs. (10)–(15)] to the upper ($u,\lvert m_j\rvert=\frac{3}{2}$) and the lower ($l,\lvert m_j\rvert=\frac{1}{2}$) sublevels of A^0 in Si under uniaxial compression are listed in the Tables I–VI. They are

TABLE IV. Relative probabilities of the optical transitions from A^0X with holes in the lowest two-hole state and electron in the specified VO state to the upper (u) and the lower (l) sublevels of A^0 split by the [111] uniaxial compression of the sample. Light is emitted perpendicular to the stress axis with polarization parallel to the stress axis.

VO state	$u(\lvert m_j'\rvert=\frac{3}{2})$	$l(\lvert m_j'\rvert=\frac{1}{2})$
$\Gamma_6(\Gamma_1)$	0	$\frac{8}{9}(1+\kappa)(2\eta+\lambda)^2$
$\Gamma_8(\Gamma_3)$	$\frac{4}{3}(1-\kappa)(\eta-\lambda)^2$	$\frac{4}{9}(1+\kappa)(\eta-\lambda)^2$
$\Gamma_7(\Gamma_5)$	0	$\frac{8}{3}(1+\kappa)\gamma^2$
$\Gamma_8(\Gamma_5)$	$\frac{4}{3}(1-\kappa)\gamma^2$	$\frac{4}{3}(1+\kappa)\gamma^2$

TABLE V. Relative probabilities of the optical transitions from A^0X with holes in the two-hole state Γ_1 and electron in the VO state $\psi^{(n)}$ to the upper (u) and the lower (l) sublevels of A^0 split by the [110] uniaxial compression of the sample. Light is emitted perpendicular to the stress axis at an angle φ with respect to the [001] axis and polarization perpendicular to the stress axis.

$\psi_e^{(n)}$	$u(\lvert m_j''\rvert=\frac{3}{2})$	$l(\lvert m_j''\rvert=\frac{1}{2})$
1σ	$\left\{\left[\sqrt{(1+\xi)}(2\eta+\lambda)+\frac{x}{\lvert x\rvert}\sqrt{2(1-\xi)}(\eta-\lambda)\right]^2\frac{4r^2}{3}\sin^2\varphi\right.$	$\left\{\left[\sqrt{(1+\xi)}(2\eta+\lambda)+\frac{x}{\lvert x\rvert}\sqrt{2(1-\xi)}(\eta-\lambda)\right]^2\frac{4}{3}\sin^2\varphi\right.$
	$+\left[\sqrt{(1+\xi)}(2\eta+\lambda)\right.$	$+\left[\sqrt{(1+\xi)}(2\eta+\lambda)\right.$
	$\left.\left.-\frac{x}{\lvert x\rvert}\sqrt{\frac{1-\xi}{2}}(\eta-\lambda)\right]^2\frac{(1+r)^2}{3}\cos^2\varphi\right\}$	$\left.\left.-\frac{x}{\lvert x\rvert}\sqrt{\frac{1-\xi}{2}}(\eta-\lambda)\right]^2\frac{(3r-1)^2}{9}\cos^2\varphi\right\}$
3σ	$\left\{\left[\frac{x}{\lvert x\rvert}\sqrt{(1-\xi)}(2\eta+\lambda)-\sqrt{2(1+\xi)}(\eta-\lambda)\right]^2\frac{4r^2}{3}\sin^2\varphi\right.$	$\left\{\left[\frac{x}{\lvert x\rvert}\sqrt{(1-\xi)}(2\eta+\lambda)-\sqrt{2(1+\xi)}(\eta-\lambda)\right]^2\frac{4}{3}\sin^2\varphi\right.$
	$+\left[\frac{x}{\lvert x\rvert}\sqrt{(1-\xi)}(2\eta+\lambda)\right.$	$+\left[\frac{x}{\lvert x\rvert}\sqrt{(1-\xi)}(2\eta+\lambda)\right.$
	$\left.\left.+\sqrt{\frac{1+\xi}{2}}(\eta-\lambda)\right]^2\frac{(1+r)^2}{3}\cos^2\varphi\right\}$	$\left.\left.+\sqrt{\frac{1+\xi}{2}}(\eta-\lambda)\right]^2\frac{(3r-1)^2}{9}\cos^2\varphi\right\}$
32	$(1-r)^2(\eta-\lambda)^2\cos^2\varphi$	$(3r-1)^2\frac{(\eta-\lambda)^2}{3}\cos^2\varphi$
$51(5z)$	$\{2(1-\zeta)\sin^2\varphi+[r\sqrt{2(1-\zeta)}-(1+r)\sqrt{1+\zeta}]\cos^2\varphi\}\gamma^2$	$\{6r^2(1-\zeta)\sin^2\varphi+\frac{1}{3}[\sqrt{2(1-\zeta)}+(3r-1)\sqrt{1+\zeta}]\cos^2\varphi\}\gamma^2$
$52(5\pm)$	$\{2(1+\zeta)\sin^2\varphi+[r\sqrt{2(1+\zeta)}+(1+r)\sqrt{1-\zeta}]\cos^2\varphi\}\gamma^2$	$\{6r^2(1+\zeta)\sin^2\varphi+\frac{1}{3}[\sqrt{2(1+\zeta)}-(3r-1)\sqrt{1-\zeta}]\cos^2\varphi\}\gamma^2$
$53(5\pm)$	$4r^2\gamma^2$	$\frac{4}{3}\gamma^2$

$$r=\frac{\Delta_{001}+2\Delta_{110}}{3\Delta_{111}}$$

$$x=-\frac{\Xi_u(S_{11}-S_{12})T}{6\Delta_{31}^{\mathrm{VO}}},\quad \xi=\frac{1+x}{\sqrt{1+2x+9x^2}},\quad y=-\frac{\Xi_u(S_{11}-S_{12})T}{6\lambda^{\mathrm{SO}}},\quad \zeta=\frac{1+6y}{3\sqrt{1+\frac{4}{3}y+4y^2}}$$

expressed in terms of three independent constants η, γ, and λ from the selection rules of Ref. 1. The relative probabilities for $\mathbf{F}\|\langle 001\rangle$ and $\mathbf{F}\|\langle 111\rangle$ were reported previously[7] without account for the mixing of the states and the SOC. The relative intensities of components in the PL spectra can be obtained by multiplying these probabilities by the relative populations of the corresponding initial states of A^0X.

Parameter κ accounts for the stress-induced mixing of the two-hole state Γ_1 with the state Γ_3 for $\mathbf{F}\|\langle 001\rangle$ or with the state Γ_5 for $\mathbf{F}\|\langle 111\rangle$. The relative probabilities of optical

TABLE VI. Relative probabilities of the optical transitions from A^0X with holes in the two-hole state Γ_1 and electron in the VO state $\psi^{(n)}$ to the upper (u) and the lower (l) sublevels of A^0 split by the [110] uniaxial compression of the sample. Light is emitted perpendicular to the stress axis with polarization parallel to the stress axis.

$\psi_e^{(n)}$	$u(\lvert m_j''\rvert=\frac{3}{2})$	$l(\lvert m_j''\rvert=\frac{1}{2})$
1σ	$\frac{(1-r)^2}{3}\left[\sqrt{(1+\xi)}(2\eta+\lambda)-\frac{x}{\lvert x\rvert}\sqrt{\frac{1-\xi}{2}}(\eta-\lambda)\right]^2$	$\frac{(3r+1)^2}{9}\left[\sqrt{(1+\xi)}(2\eta+\lambda)-\frac{x}{\lvert x\rvert}\sqrt{\frac{1-\xi}{2}}(\eta-\lambda)\right]^2$
3σ	$\frac{(1-r)^2}{3}\left[\frac{x}{\lvert x\rvert}\sqrt{(1-\xi)}(2\eta+\lambda)+\sqrt{\frac{1+\xi}{2}}(\eta-\lambda)\right]^2$	$\frac{(3r+1)^2}{9}\left[\frac{x}{\lvert x\rvert}\sqrt{(1-\xi)}(2\eta+\lambda)+\sqrt{\frac{1+\xi}{2}}(\eta-\lambda)\right]^2$
32	$(1+r)^2(\eta-\lambda)^2$	$\frac{(3r+1)^2}{3}(\eta-\lambda)^2$
$51(5z)$	$[r\sqrt{2(1-\zeta)}+(1-r)\sqrt{1+\zeta}]\gamma^2$	$\frac{1}{3}[\sqrt{2(1-\zeta)}-(3r+1)\sqrt{1+\zeta}]\gamma^2$
$52(5\pm)$	$[r\sqrt{2(1+\zeta)}-(1-r)\sqrt{1-\zeta}]\gamma^2$	$\frac{1}{3}[\sqrt{2(1+\zeta)}+(3r+1)\sqrt{1-\zeta}]\gamma^2$
$53(5\pm)$	$4r^2\gamma^2$	$\frac{4}{3}\gamma^2$

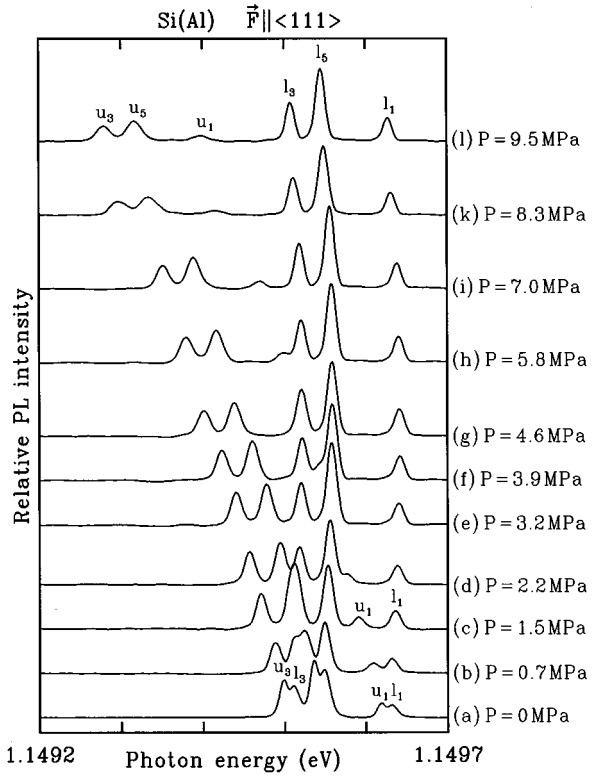

FIG. 2. PL spectra of excitons bound to Al acceptors (Al^0X) under ⟨111⟩ compressive stress P shown on the right-hand side beside each spectrum increasing from (b) to (l). Bath temperature $T=2$ K, resolution 0.0025 meV. Transitions to the upper or lower sublevels of the acceptor are labeled by the letter u or l, respectively, with the subscript corresponding to the label of the A^0X energy level in Fig. 1. The relative amplitudes of the peaks (for instance, u_1 and l_1) change rapidly from (a) to (b) and then remain relatively constant with slow decline of the u components due to the modification of the two-hole state of Al^0X.

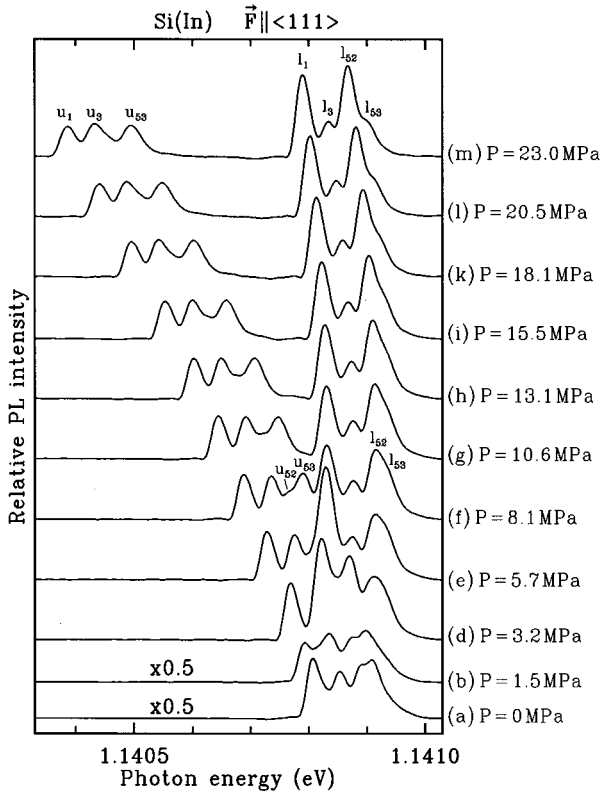

FIG. 3. PL spectra of excitons bound to In acceptors (In^0X) under ⟨111⟩ stress increasing from (b) to (m). $T=2$ K, resolution 0.006 meV. The relative amplitudes of the components 52 and 53 for the transitions to the upper (u) and lower (l) sublevels of the acceptor are consistent with the assignment of these components to the Γ_5 VO states of In^0X split by SOC which explains the presence of the fourth peak in the zero-stress spectrum (a). The relative amplitudes of the peaks change rapidly from (a) to (d) and then remain relatively constant. Small increase of the splitting between the components 1_{52} and 1_{53} and change in their relative amplitudes from (g) to (m) is, probably, due to small deviation of the stress axis from ⟨111⟩.

transitions for $\mathbf{F}\|\langle 110\rangle$ were obtained only for the Γ_1 two-hole state because the ⟨110⟩ strains mix it with both the Γ_3 and the Γ_5 states in a more complicated manner. This mixing, however, is not important if $\tilde{\Delta}\ll\Delta_{31}^{hh}$ and $\tilde{\Delta}\ll\Delta_{51}^{hh}$.

Probabilities of the transitions from the A^0X states $\psi^{(1\sigma)}$ and $\psi^{(3\sigma)}$ [Eqs. (10) and (11)] depend on the ratio $x\equiv\sigma/\Delta_{31}^{VO}$ of the stress-induced splitting of the conduction band $\Delta_c=3\sigma$ and the zero stress splitting Δ_{31}^{VO} between the VO states Γ_3 and Γ_1. This dependence is accounted for by the parameter $\xi=(1+x)/(\sqrt{1+2x+9x^2})$ [Eqs. (10) and (11)] which is equal to 1 at zero stress and to $\pm\frac{1}{3}$ in the limit of infinite stress. The parameter ζ [Eqs. (13) and (14)] accounts in a similar manner for the stress-induced mixing of the Γ_5 VO states when SOC is not negligible. $\zeta=\frac{1}{3}$ at zero stress and ±1 when $|\lambda^{SO}|\ll|\Delta_c|$.

The eigenfunctions of A^0 for $\mathbf{F}\|\langle 110\rangle$ depend on the ratio $r=[(\Delta_{001}+2\Delta_{110})/3\Delta_{111}]$ [Eq. (2)] and so do the probabilities of optical transitions.[14] If $\Delta_{001}=\Delta_{111}$, $r=1$, and the stress-induced splitting of A^0, Δ, does not depend on the stress direction. Deviation of r from 1 is a measure of the anisotropy of Δ. The probability of emitting light with polarization perpendicular to the [110] stress axis depends also on the angle φ between the direction in which light is emitted from the sample and the [001] axis. For example, component (32) must completely vanish for $\varphi=90°$.

III. EXPERIMENT

A. Experimental techniques

The samples were made from a high-purity float-zone silicon doped with Al, Ga, In, and Tl in concentrations from 10^{14} to 2×10^{15} cm^{-3}. The Al-, Ga-, and In-doped samples had a shape of a $2\times2\times20$ mm^3 parallelepiped with long sides x-ray oriented along one of the ⟨111⟩, ⟨110⟩, or ⟨001⟩ crystallographic directions and the ends shaped as square pyramids.[2] They were mounted in a stress rig with the tops of the pyramids on either end of the sample placed in small conical dips punched in the exact middle of opposing cylindrical brass pistons, thus ensuring precise alignment of the sample.[2] Due to the limited quantity of the material, the Tl doped samples have been made in a shape of a $2\times4\times0.5$ mm^3 parallelepiped with the long side x-ray oriented along the ⟨001⟩ or ⟨110⟩ directions. They were mounted between two lead gaskets in order to produce a homogeneous strain in the sample.

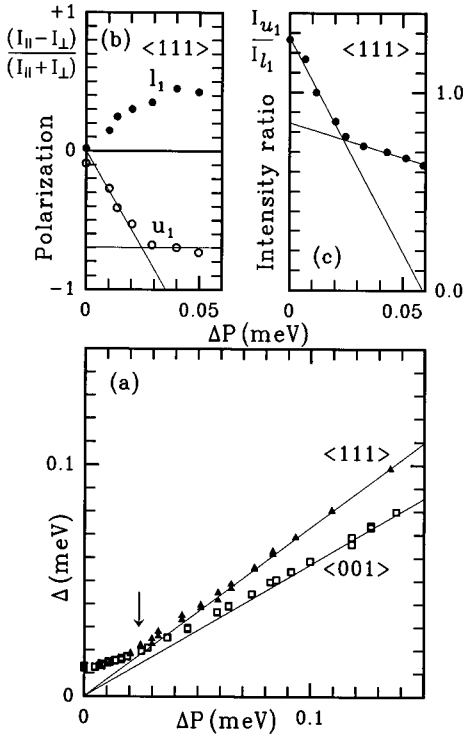

FIG. 4. Splitting Δ between the components u_1 and l_1 (a) in the PL spectra of Al^0X under small $\langle 111\rangle$ stress, the degree of their polarization (b) and the amplitude ratio (c) as a function of the splitting, ΔP, of the narrow (FWHM=0.006 meV) line of excitons bound to residual phosphorous donors proportional to the stress. Rapid but gradual changes of polarizations (b) and relative amplitudes (c) occur in the small stress range marked by an arrow on (a) while Δ remains within 1.5 of its zero stress value Δ_0.

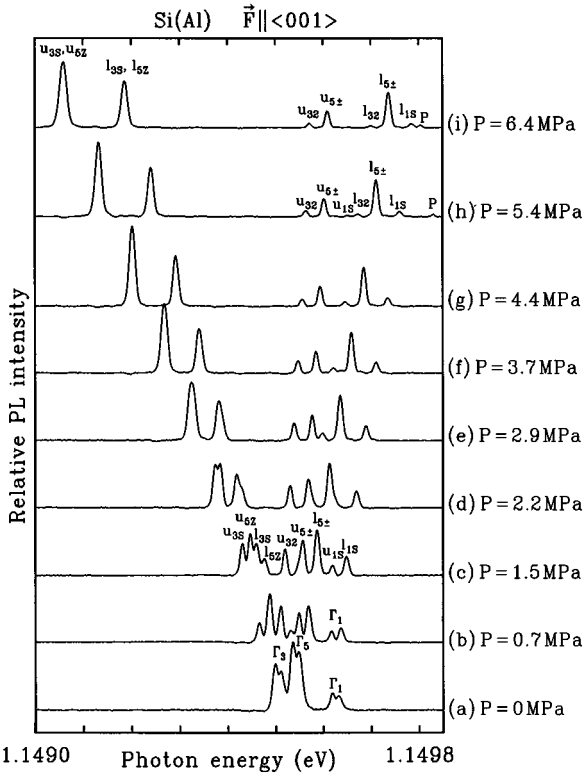

FIG. 5. PL spectra of Al^0X under $\langle 001\rangle$ stress increasing from (b) to (i) at $T=2$ K and 0.0025 meV resolution. Zero-stress doublets Γ_3 and Γ_5 (a) split at much higher rates (b) than the doublet Γ_1, yet, have the same width and line shape at zero stress as Γ_1. Label P marks the PL of excitons bound to the residual phosphorous donors.

The stress rig with the sample mounted was immersed in a pumped liquid-He bath, and the sample was photoexcited with a 0.5-W cw 0.98-μm wavelength Ti-sapphire laser beam. The near-infrared luminescence radiation emitted from the sample was analyzed by BOMEM DA8 Michelson interferometer fitted with a 77-K Ge photodetector (North Coast). Interferograms of luminescence from the sample were Fourier-transformed into PL spectra with a resolution of up to 0.0025 meV.

B. PL spectra of A^0X in Si under uniaxial stress

Figures 2 and 3 show the PL spectra of Al^0X and In^0X in Si under uniaxial compression (stress $P=-T>0$) in the $\langle 111\rangle$ crystallographic direction. (It should be noted that, due to a small calibration error, the absolute energy scale in Ref. 1 should be shifted downwards by 0.068 meV.) We did not have enough material to make a Tl-doped sample with the $\langle 111\rangle$ orientation, and we do not show the PL spectra of Ga^0X since they are similar to those of Al^0X except for the different magnitude of the VOS. We label the components in the spectra by a letter u for the transitions to the upper sublevel of A^0 and l for the transitions to the lower sublevel. The subscripts on the labels indicate the VO states of the electron in A^0X and are identical to the corresponding subscripts in the notation of the single-electron energy levels [Eqs. (10)–(15)].

For $\mathbf{F}\|\langle 111\rangle$, $\cos^2\theta=\frac{1}{3}$ and, as follows from Eq. (8), the stress in $\langle 111\rangle$ direction does not affect the VOS and SOC in A^0X. The PL spectrum under $\langle 111\rangle$ stress contains two sets of triplets in the case of Al^0X ($\lambda^{SO}=0$) or two sets of quadruplets in the case of In^0X ($\lambda^{SO}\neq 0$), which move apart with increasing P but do not change the separation of the components or their relative amplitudes while the stress-induced splitting Δ between the upper (u) and the lower (l) sublevels of A^0 is much greater than the intrinsic zero-stress splitting Δ_0. (The slight increase of the splitting between the components 52 and 53 in the PL spectra of In^0X and the gradual change of their relative amplitudes above 15 MPa are, probably, due to small deviation of the stress axis from the $\langle 111\rangle$ direction.)

The dependence of Δ on P (Fig. 4) is linear when $\Delta \gg \Delta_0$, and nonlinear when $\Delta\sim\Delta_0$. To achieve better accuracy, the stress in Fig. 4 was calibrated according to the linear splitting ΔP of the narrow (FWHM$\approx$0.006 meV) line of excitons bound to residual phosphorous donors. Rapid changes of the relative amplitudes and polarizations of the components occur in a very small range of P where $\Delta \leqslant \sqrt{2}\Delta_0$ (marked with an arrow in Fig. 4). This behavior implies strong mixing of the zero-stress A^0 states and can be explained in the Jahn-Teller effect model of the intrinsic ground-state splitting[8,10,11] Δ_0 by a gradual decoupling of the vibronic states due to removal of electronic degeneracy by the strain. Similar effects of very small strains on the PL spectra have been observed for In.

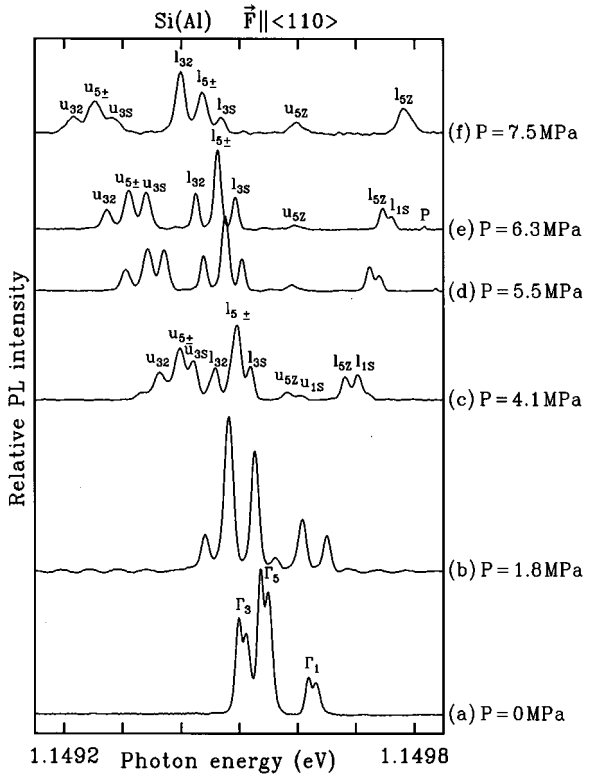

FIG. 6. PL spectra of Al^0X under ⟨110⟩ stress increasing from (b) to (f). $T=2$ K, resolution 0.0025 meV for (a)–(e) and 0.006 meV for (f). PL radiation was emitted from the sample in the ⟨110⟩ direction for (b)–(e) and the ⟨001⟩ direction for (f) resulting in different amplitude ratios for (e) and (f). Separation between the components $l_{3\sigma}$ and l_{5z}, l_{1S} and $l_{5\pm}$, $u_{1\sigma}$ and $u_{5\pm}$ changes from (c) to (e) due to the mixing of the VO states 3σ and 1σ.

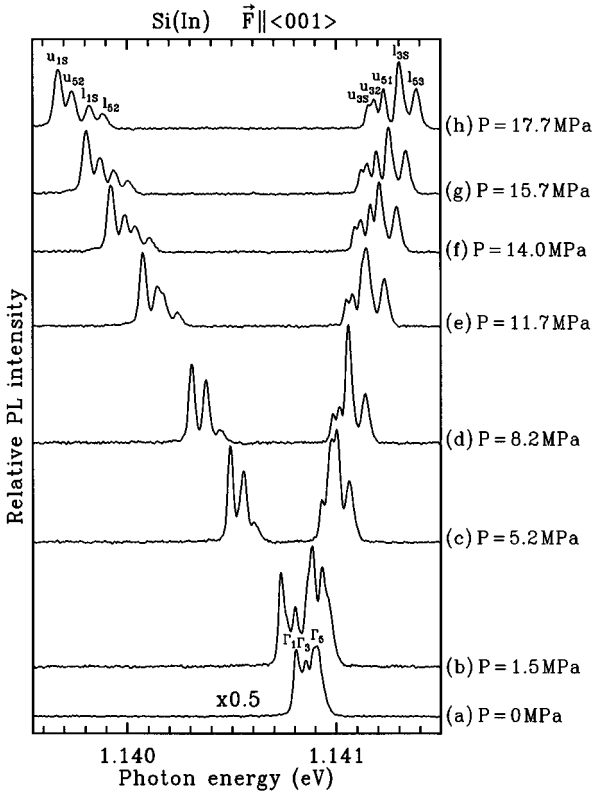

FIG. 7. PL spectra of In^0X under ⟨001⟩ stress increasing from (b) to (h) at $T=2$ K and 0.006 meV resolution. The rate of the stress-induced splitting of In^0 equal to the separation between the corresponding l and u components is less than one half of that for the ⟨111⟩ stress (Fig. 3).

For $\mathbf{F}\|\langle 001\rangle$ and $\mathbf{F}\|\langle 110\rangle$ (Figs. 5–10), $\sigma\neq 0$ in Eq. (8), and the strain splits the electron states in A^0X and changes VOS and SOC (Fig. 1). The spectrum for these stress directions consists of up to 12 well-resolved components and undergoes complex transformations with the stress that can be accounted for by the theoretical model outlined in the previous section. PL components due to the excited VO states of A^0X persist in the spectra even when the stress-induced splitting of the conduction band $\Delta_c \gg kT$, indicating that the VO states are typically not in thermal equilibrium at the lattice temperature.[3] For Tl, these components gradually vanish from the spectra when Δ_c is increased from 0 to ≈ 2.5 meV and then reappear again at higher stresses (Figs. 9 and 10).

Experimental positions of the PL peaks as a function of the uniaxial stress in ⟨001⟩, ⟨111⟩, and ⟨110⟩ directions are shown by small solid circles on the fan charts in Figs. 11–14. Curved solid lines in this charts represent theoretical peak positions calculated from Eqs. (2)–(6) and (8)–(15). The VO splittings $\Delta_{15}^{\mathrm{VO}}$, $\Delta_{35}^{\mathrm{VO}}$ and the SOC constant λ^{SO} were determined directly from the zero-stress PL spectra in Ref. 1. The deformation potential constants b, d, and Ξ_u listed in the Table VII were determined from the best fit to the subset of data for the ⟨001⟩ and ⟨111⟩ stress directions with an estimated accuracy of about 2% for Al^0, Ga^0, and In^0. Uncertainty in the values of b and d is much greater for A^0X since these values affect only the nonlinear shift ΔE^{hh} of all PL components given by Eqs. (3)–(5) with the experimental val-

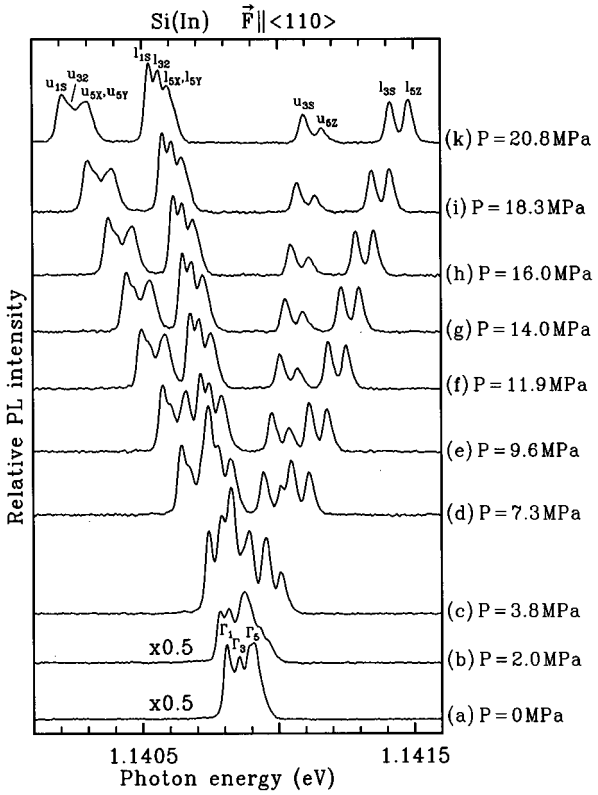

FIG. 8. PL spectra of In^0X under ⟨110⟩ stress increasing from (b) to (k) at $T=2$ K and 0.006 meV resolution.

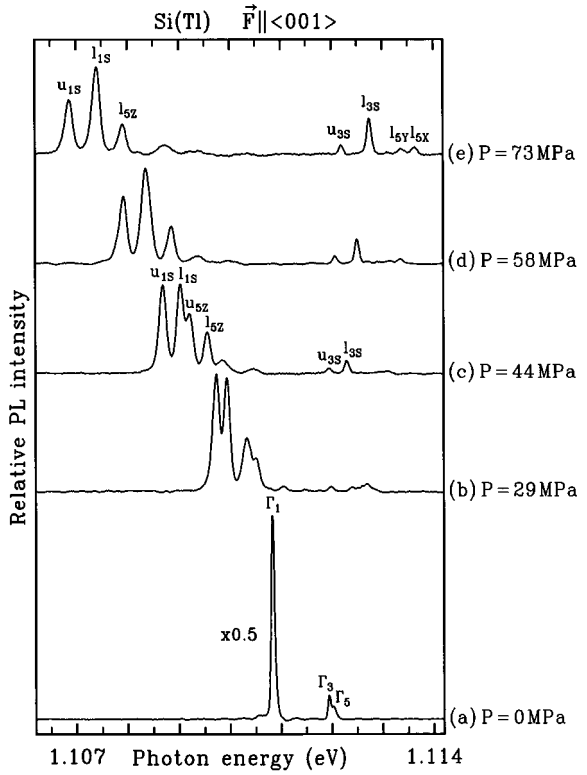

FIG. 9. PL spectra of Tl^0X under $\langle 001\rangle$ stress increasing from (b) to (e) at $T=2$ K and 0.03 meV resolution. Components l_{5x} and l_{5y} are slightly split on (e) due to small deviation of the stress axis from $\langle 001\rangle$. Components $u_{3\sigma}$, $l_{3\sigma}$, l_{5x}, and l_{5y} corresponding to the excited VO states of Tl^0X thermalize strongly at 29 MPa (b) but gradually reemerge at higher stresses (c)–(e).

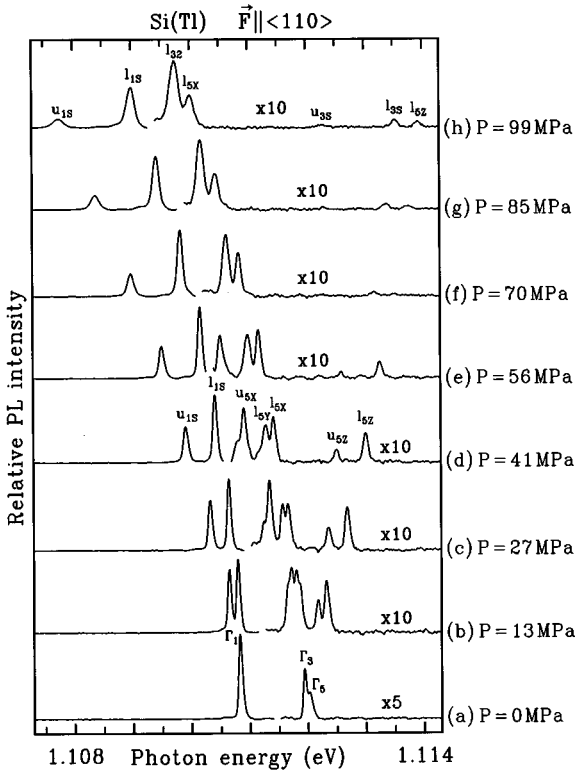

FIG. 10. PL spectra of Tl^0X under $\sim\langle 110\rangle$ stress increasing from (b) to (h) at $T=2$ K and 0.03 meV resolution. Components l_{5x} and l_{5y} are slightly split due to small deviation of the stress axis from $\langle 110\rangle$. Components $u_{3\sigma}$, $l_{3\sigma}$, and l_{5y} corresponding to the excited VO states of Tl^0X gradually thermalize from (b) to (f) but then reemerge at higher stresses on (g) and (h).

ues of the parameters Δ_{31}^{hh} and Δ_{51}^{hh} taken from Refs. 15–17. A lower (about 10%) accuracy of b and d for Tl^0, which were obtained from the best fit to the $\langle 001\rangle$ and $\langle 110\rangle$ data, is due to the less accurate stress calibration and small misalignment of the samples.

The pattern of the stress-induced splittings and the nonlinear relative shifts of the components depend uniquely on the zero-stress VOS and SOC. The zero-stress components can be identified unambiguously from the pattern of the fan charts shown in Figs. 11–14. In particular, the three peaks in the zero-stress spectra of Tl^0X must be attributed to the VO states Γ_1, Γ_3, and Γ_5 of Tl^0X with holes in the $J=0$ state. Due to the small misalignment of the Tl-doped samples in the stress rig, the stress was applied in directions slightly different from $\langle 001\rangle$ and $\langle 110\rangle$. As a result, the x and y minima of the conduction band had slightly different energies and the PL components $5x$ and $5y$, which otherwise would be degenerate, were split under the stress. Theoretical curves in Fig. 14 account for the small deviation of the stress axis from the $\langle 001\rangle$ or $\langle 110\rangle$ direction which was represented in the calculations for Tl by an additional adjustable parameter. The observed splitting between the $5x$ and $5y$ PL components can be explained only if the zero-stress VO state Γ_5 has a higher energy than the state Γ_3.

The zero-stress PL component Γ_1 splits under small $\langle 001\rangle$ stress at a much slower rate than the components Γ_3 and Γ_5. If the doublet structure of these components observed at zero stress for Al^0X (Refs. 10 and 11 and Figs. 2, 5, and 6) was due to some randomly distributed elastic strains in the sample, one would expect that these elastic strains would split or broaden the Γ_3 and Γ_5 components to a greater extent than the component Γ_1. However, as was shown in Ref. 1, and in Fig. 2(a), the line shape and the width of these components is identical, thus confirming once again that this doublet structure is due to an intrinsic splitting Δ_0 rather than to random strains.

C. Polarizations and the amplitude ratios in the PL spectra of A^0X under uniaxial compression

The theoretical model developed in this work allows us to predict positions of the PL peaks and their relative amplitudes and polarizations for the $\langle 001\rangle$, $\langle 111\rangle$, and $\langle 110\rangle$ stress directions. It does not describe the line shape of the PL components, but one can assume that all the components have the same line shape which can be approximated by a combination of the Gaussian and the Lorentzian line shapes. Convolution of this fixed line shape with the δ functions corresponding to the PL peaks produced realistic theoretical spectra of A^0X (Figs. 15–18) very similar to experimental spectra. Theoretical spectra were calculated without any further adjustable parameters except for the effective temperature T^{eff} accounting for deviation of the population of the excited VO states from thermal equilibrium at the liquid-He bath temperature T. The ratios of the constants λ/η and γ/η

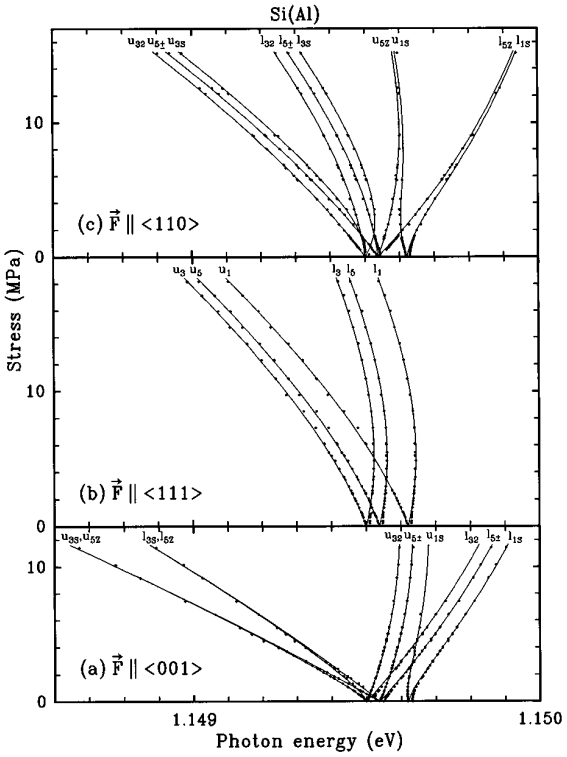

FIG. 11. Experimental (dots) and theoretical (solid lines) positions of the Al^0X PL peaks as a function of uniaxial stress in ⟨001⟩ (a), ⟨111⟩ (b), and ⟨110⟩ (c) directions. Significant deviations of the theory from the experiment occur only for very small stress values when the stress-induced splitting, Δ [Eq. (2)], of Al^0 is comparable with the intrinsic zero-stress splitting Δ_0.

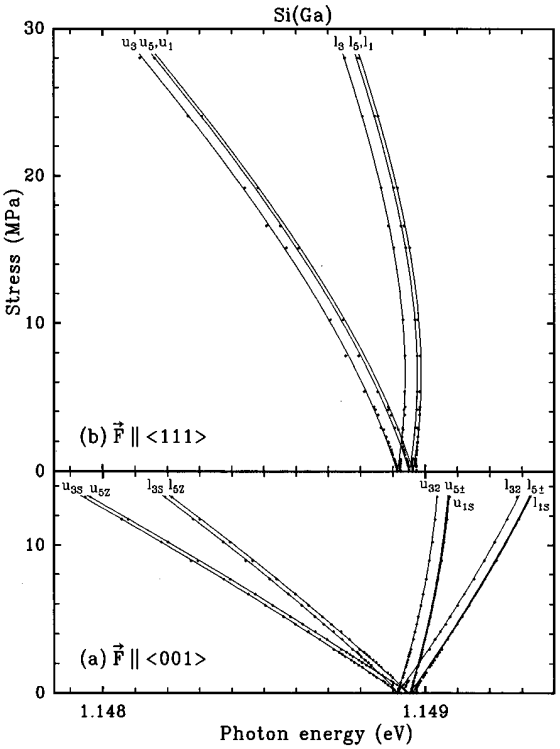

FIG. 12. Experimental (dots) and theoretical (solid lines) positions of the Ga^0X PL peaks as a function of uniaxial stress in ⟨001⟩ (a) and ⟨111⟩ (b) directions.

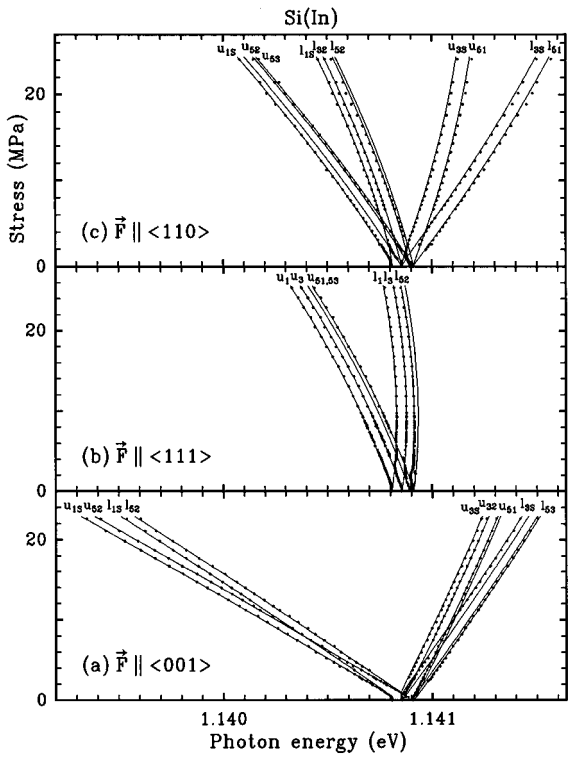

FIG. 13. Experimental (dots) and theoretical (solid lines) positions of the In^0X PL peaks as a function of uniaxial stress in ⟨001⟩ (a), ⟨111⟩ (b), and ⟨110⟩ (c) directions.

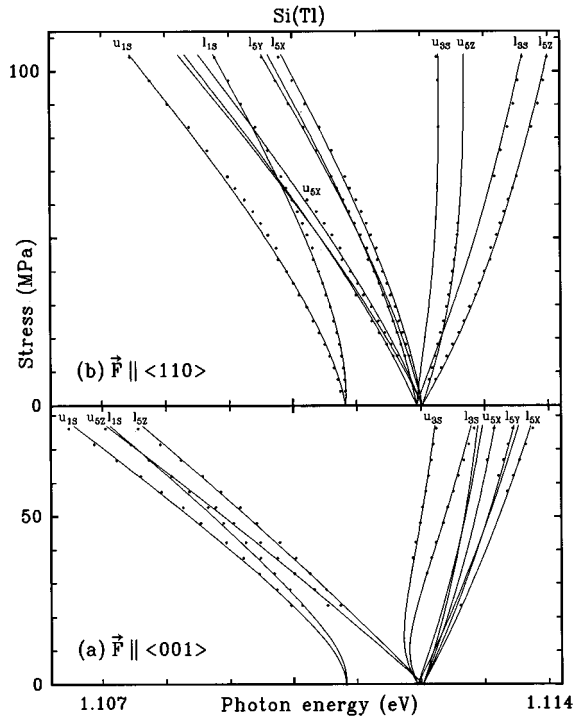

FIG. 14. Experimental (dots) and theoretical (solid lines) positions of the Tl^0X PL peaks as a function of uniaxial stress in $\sim\langle 001\rangle$ (a) and $\sim\langle 110\rangle$ directions. Components l_{5x} and l_{5y} are slightly split due to small deviations of the stress axis from ⟨001⟩ and ⟨110⟩, respectively.

TABLE VII. Deformation-potential constants for the group III A^0 and A^0X in eV, and the A^0 anisotropy parameter $r=[(\Delta_{001}+2\Delta_{110})/3\Delta_{111}]$ (deviation of r from 1 characterizes anisotropy of the stress-induced splitting of A^0).

Acceptor	B	Al	Ga	In	Tl
$\Xi_d+\frac{1}{3}\Xi_u+2a(A^0X)-a(A^0)$		0.9 ± 0.2	1.0 ± 0.2	1.2 ± 0.3	0.8 ± 0.3
$b(A^0)$	-1.35 ± 0.05[a]	-1.01 ± 0.02	-1.03 ± 0.02	-0.43 ± 0.01	-0.30 ± 0.03
$d(A^0)$	-3.95 ± 0.1[a]	-3.31 ± 0.06	-3.10 ± 0.06	-2.41 ± 0.05	-1.95 ± 0.2
$b(A^0X)$	-1.49 ± 0.05[a]	-1.5 ± 0.2	-1.5 ± 0.2	-1.2 ± 0.3	-0.8 ± 0.3
$d(A^0X)$	-4.08 ± 0.1[a]	-4.5 ± 0.6	-4.1 ± 0.6	3.9 ± 1.0	-3.3 ± 1.2
$\Xi_u(A^0X)$	8.5 ± 0.2[a]	8.71 ± 0.15	8.60 ± 0.15	8.66 ± 0.15	8.5 ± 0.8
r	0.963	0.915	0.925	0.760	0.733

[a]After Karasyuk *et al.* (Ref. 9).

that govern the relative amplitudes of the PL peaks were taken from Ref. 1. The deformation-potential constants and the quantities that can be derived from them, such as the parameters κ, ξ, ζ, and r had been already determined independently. Only for Tl, the ratios $\lambda/\eta=0.5$ and $\gamma/\eta=0.9$ have been adjusted in order to produce a better agreement with the experiment. The previous values for Tl ($\lambda/\eta=-0.1$ and $\gamma/\eta=0.6$) were determined from the zero-field spectrum of Ref. 1 with large uncertainty (apparently, greater than was estimated) because of the partial thermalization of the excited VO orbit states.

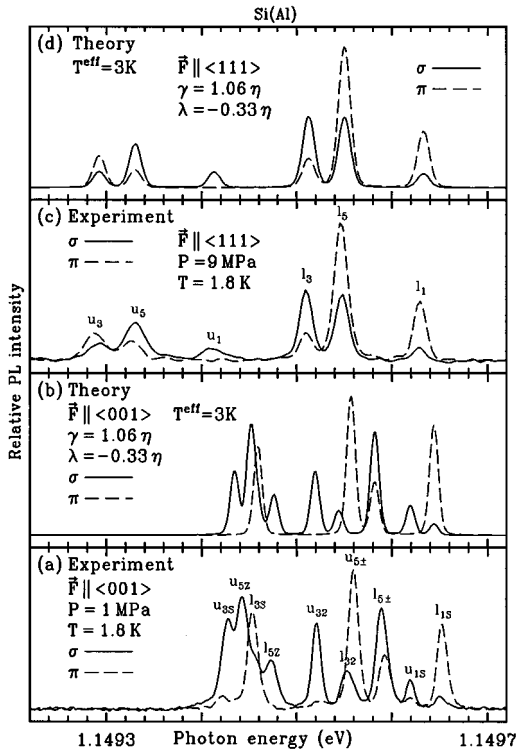

FIG. 15. Experimental [(a) and (c)] and theoretical [(b) and (d)] PL spectra of Al^0X polarized perpendicular (σ) and parallel (π) to the stress axis for the $\langle001\rangle$ [(a) and (b), $P=1$ MPa] and $\langle111\rangle$ [(a) and (c), $P=9$ MPa] stress. The theoretical spectra (b) and (d) present convolution of twelve Gaussian peaks centered at the photon energies determined from [Eqs. (2)–(5), (7)–(14)] with relative amplitudes listed in Tables I–IV. Thermal equilibrium is assumed for (b) and (d) between the Al^0X VO states at the effective temperature $T^{eff}=3$ K.

The theoretical spectra agree very well with the experiment taking into account ~10% depolarization in experimental PL spectra, nonthermal population of the excited VO states of A^0X, and that the luminescence is emitted over a range of angles rather than in one specific direction, which is particularly significant for $\mathbf{F}\|\langle110\rangle$. All the components have the correct polarizations and the relative amplitudes are close to experimental. The degree of polarization thus provides a reliable method of identification of the components. Good agreement between the theoretical and the experimental PL spectra confirms the correctness of the assignment of the VO states to the zero-stress components.

A special feature of the selection rules for $\mathbf{F}\|\langle110\rangle$ is that the relative probabilities of the optical transitions strongly depend on the direction in which luminescence light is emitted from the sample (Table V). We observed this dependence

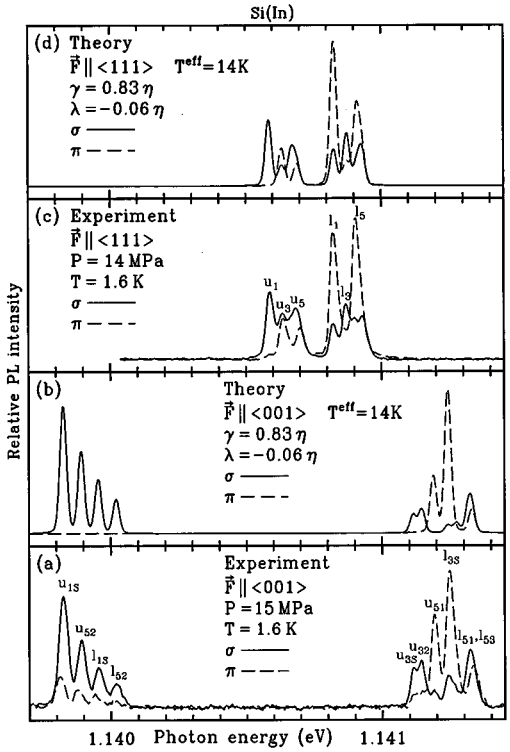

FIG. 16. Experimental [(a) and (c)] and theoretical [(b) and (d)] PL spectra of In^0X polarized perpendicular (σ) and parallel (π) to the stress axis for the $\langle001\rangle$ [(a) and (b), $P=15$ MPa] and $\langle111\rangle$ [(c) and (d), $P=14$ MPa] stress. $T^{eff}=14$ K for (b) and (d).

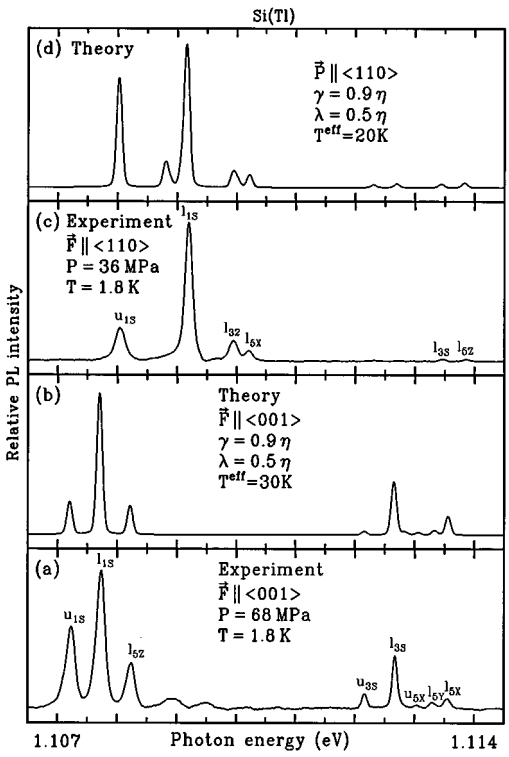

FIG. 17. Experimental [(a) and (c)] and theoretical [(b) and (d)] PL spectra of Tl^0X for the $\sim\langle 001\rangle$ [(a) and (b), $P=68$ MPa] and $\sim\langle 110\rangle$ [(c) and (d), $P=36$ MPa] stress. $T^{\rm eff}=30$ K for (b) and 20 K for (d). Components l_{5x} and l_{5y} are slightly split on (a) and (b) due to small deviation of the stress axis from $\langle 110\rangle$.

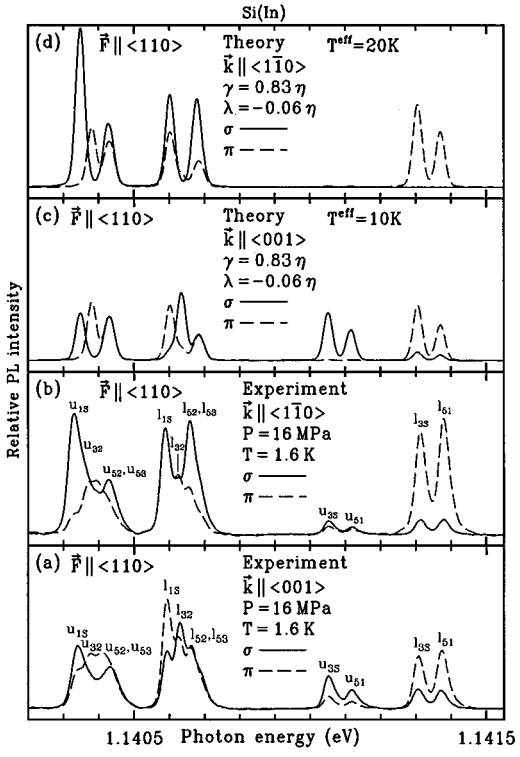

FIG. 18. Experimental [(a) and (b)] and theoretical [(c) and (d)] PL spectra of In^0X polarized perpendicular (σ) and parallel (π) to the stress axis for the $\langle 110\rangle$ stress $P=16$ MPa. The experimental spectra were recorded in otherwise identical conditions for PL radiation emitted from the sample in $\langle 110\rangle$ (a) or $\langle 001\rangle$ (b) directions. $T^{\rm eff}=10$ K for (c) and 30 K for (d).

experimentally for In by recording the PL spectra in identical conditions except that in one case the luminescence was collected perpendicular to the (001) plane, and in another perpendicular to the (110) plane [Figs. 18(a) and 18(b)]. The theory predicts, for instance, that the components u_{32} and u_{51} that are quite strong in the luminescence emitted in the $\langle 001\rangle$ direction [Fig. 18(c)] should disappear in the luminescence emitted in the $\langle 110\rangle$ direction [Fig. 18(d)]. Indeed the relative intensity of these components drops dramatically when the sample is merely rotated by 90° about the stress axis. Discrepancies between the theoretical and the experimental spectra in Fig. 18 are probably due to the finite size of the solid angle from which the light was collected, and to multiple internal reflections and scattering of the light within the sample. The significant dependence of the observed spectrum on the angle of observation can be seen as well in the In^0X spectra recorded without any polarizer (Fig. 19).

IV. DISCUSSION

The results of our uniaxial stress experiments confirm that our theoretical model which is based essentially on the Hartree-Fock approximation and the effective-mass approximation adequately describes A^0X not only for the shallow acceptors such as Al or Ga, but also for the deeper In and even for the very deep Tl (ionization and binding energies are listed in Table V of Ref. 1). They reaffirm that in the ground state of A^0X holes occupy the $J=0$ two-hole state for all the group-III acceptors with the possible exception of B^0X, where the relatively weak j-j coupling of holes is comparable with the electron-hole coupling. Good agreement between the theory and the experiment ascertains that the quadruplet fine structure of In^0X is due to the valley-orbit splitting and the spin-orbit coupling of the Γ_5 VO states. We also determined from our experiments the ordering of the VO states in Tl^0X as $\Gamma_1,\Gamma_3,\Gamma_5$ with energy increasing from Γ_1 to Γ_5.

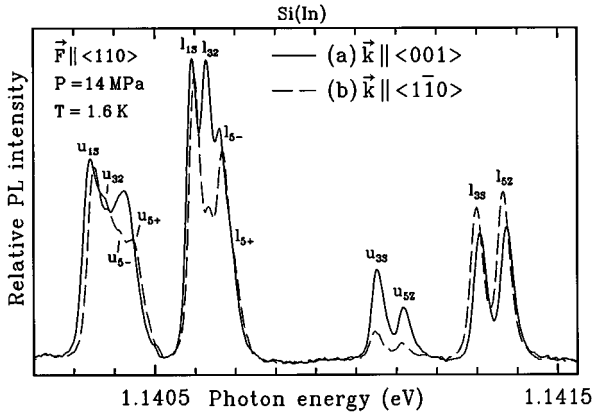

FIG. 19. PL spectra of In^0X for the $\langle 110\rangle$ stress $P=14$ MPa recorded in otherwise identical conditions for PL radiation emitted from the sample in $\langle 001\rangle$ (a) and $\langle 110\rangle$ (b) directions.

A high-precision uniaxial stress technique[2] has allowed us to measure the deformation-potential constants for Al^0, Ga^0, and In^0 with a very high accuracy of $\sim 2\%$. Unfortunately, we could not use this technique for Tl due to the small amount of the Tl-doped material, however, we were able to determine the deformation-potential constants for Tl^0, to the best of our knowledge not available in the literature prior to the present paper, with an estimated accuracy of $\sim 10\%$. The deformation-potential constants b and d decrease monotonically from B to Tl with the increase of the acceptor ionization energy. This decrease is more pronounced for A^0 than for A^0X, and is about twice as strong for b as it is for d. On the other hand, the deformation potential Ξ_u of the electron in A^0X is the same for all group-III acceptors in Si within experimental error. The anisotropy parameter $r=[(\Delta_{001}+2\Delta_{110})/3\Delta_{111}]$ is close to 1 for B, which means that the strain-induced splitting of A^0 is almost independent of the strain direction. Deviation of r from 1 indicates anisotropy of this splitting, which gets progressively stronger for the deeper acceptors, implying stronger anisotropy of the A^0 states.

No significant deviations of experimental spectra from the theoretical predictions have been observed except for the very low-stress data, where the stress-induced splitting of A^0 is smaller than the intrinsic ground-state splitting. Rapid changes that occur in the relative amplitudes and polarizations of the PL components while their positions remain almost the same under very small strains are consistent with the assumption that the intrinsic ground-state splitting is produced by a dynamic Jahn-Teller effect.[8,10,11]

ACKNOWLEDGMENTS

This work was supported partly by the Natural Sciences and Engineering Research Council of Canada and by the Science and Engineering Research Council (United Kingdom).

[1] V. A. Karasyuk, S. An, M. L. W. Thewalt, E. C. Lightowlers, and A. S. Kaminskii, Phys. Rev. B **54**, 10 543 (1996).

[2] A. S. Kaminskii, V. A. Karasyuk, and Ya. E. Pokrovskii, Zh. Eksp. Teor. Fiz. **83**, 2237 (1982) [Sov. Phys. JETP **56**, 1295 (1983)].

[3] V. D. Kulakovskii, G. E. Pikus, and V. B. Timofeev, Usp. Fiz. Nauk **135**, 237 (1981) [Sov. Phys. Usp. **24**, 815 (1981)].

[4] M. L. W. Thewalt, in *Excitons*, edited by E. I. Rashba and M. D. Sturge (North-Holland, Amsterdam, 1982), p. 393.

[5] J. Weber, H. Conzelman, and R. Sauer, in *Proceedings of the Fifteenth International Conference on the Physics of Semiconductors, Kyoto, 1980* [J. Phys. Soc. Jpn. Suppl. A **49**, 425 (1980)].

[6] V. A. Karasyuk and Ya. E. Pokrovskii, Pis'ma Zh. Eksp. Teor. Fiz. **37**, 537 (1983) [JETP Lett. **37**, 640 (1983)].

[7] M. V. Gorbunov, A. S. Kaminskii, and A. N. Safonov, Zh. Eksp. Teor. Fiz. **94**, 247 (1988) [Sov. Phys. JETP **67**, 355 (1988)].

[8] A. S. Kaminskii and A. N. Safonov, Pis'ma Zh. Eksp. Teor. Fiz. **55**, 245 (1992) [JETP Lett. **55**, 242 (1992)].

[9] V. A. Karasyuk, A. G. Steele, A. Mainwood, E. C. Lightowlers, G. Davies, M. L. W. Thewalt, and D. M. Brake, Phys. Rev. B **45**, 11 736 (1992).

[10] V. A. Karasyuk, S. An, M. L. W. Thewalt, and E. C. Lightowlers, Phys. Rev. Lett. **73**, 2340 (1994).

[11] V. A. Karasyuk, S. An, M. L. W. Thewalt, E. C. Lightowlers, and A. S. Kaminskii, Solid State Commun. **93**, 379 (1995).

[12] A. K. Ramdas and S. Rodrigues, Rep. Prog. Phys. **44**, 1297 (1981).

[13] J. J. Hall, Phys. Rev. **161**, 756 (1967).

[14] S. Rodriguez, P. Fisher, and F. Barra, Phys. Rev. B **6**, 2219 (1972).

[15] M. L. W. Thewalt, Can. J. Phys. **55**, 1463 (1977).

[16] K. R. Elliott, G. C. Osbourn, D. L. Smith, and T. C. McGill, Phys. Rev. B **17**, 1808 (1978).

[17] K. R. Elliott, D. L. Smith, and T. C. McGill, Solid State Commun. **27**, 317 (1978).